



# Magnetic microbubble mediated chemo-sonodynamic therapy using a combined magnetic-acoustic device

Estelle Beguin<sup>a,1</sup>, Michael D. Gray<sup>a,1</sup>, Keiran A. Logan<sup>b,1</sup>, Heather Nesbitt<sup>b</sup>, Yingjie Sheng<sup>b</sup>, Sukanta Kamila<sup>b</sup>, Lester C. Barnsley<sup>c</sup>, Luca Bau<sup>a</sup>, Anthony P. McHale<sup>b,\*</sup>, John F. Callan<sup>b,\*</sup>, Eleanor Stride<sup>a,\*</sup>

<sup>a</sup> Institute of Biomedical Engineering, University of Oxford, Oxford OX3 7DQ, UK

<sup>b</sup> Biomedical Sciences Research Institute, University of Ulster, Coleraine, Northern Ireland BT52 1SA, UK

<sup>c</sup> Jülich Centre for Neutron Science at Heinz Maier-Leibnitz Zentrum, Forschungszentrum Jülich GmbH, 85748 Garching, Germany

## ARTICLE INFO

### Keywords:

Microbubbles  
Drug delivery  
Magnetic targeting  
Sonodynamic therapy  
Ultrasound  
Medical devices

## ABSTRACT

Recent pre-clinical studies have demonstrated the potential of combining chemotherapy and sonodynamic therapy for the treatment of pancreatic cancer. Oxygen-loaded magnetic microbubbles have been explored as a targeted delivery vehicle for this application. Despite preliminary positive results, a previous study identified a significant practical challenge regarding the co-alignment of the magnetic and ultrasound fields. The aim of this study was to determine whether this challenge could be addressed through the use of a magnetic-acoustic device (MAD) combining a magnetic array and ultrasound transducer in a single unit, to simultaneously concentrate and activate the microbubbles at the target site. *in vitro* experiments were performed in tissue phantoms and followed by *in vivo* treatment of xenograft pancreatic cancer (BxPC-3) tumours in a murine model. *In vitro*, a 1.4-fold ( $p < .01$ ) increase in the deposition of a model therapeutic payload within the phantom was achieved using the MAD compared to separate magnetic and ultrasound devices. *In vivo*, tumours treated with the MAD had a 9% smaller mean volume 8 days after treatment, while tumours treated with separate devices or microbubbles alone were respectively 45% and 112% larger. This substantial and sustained decrease in tumour volume suggests that the proposed drug delivery approach has the potential to be an effective neoadjuvant therapy for pancreatic cancer patients.

## 1. Introduction

Microbubbles (MB) and ultrasound (US) are in routine clinical use for diagnostic imaging, and are being actively investigated for a range of therapeutic applications including in recent clinical trials for cancer treatment [1,2]. MBs consist of gas cavities 1–10 µm in diameter stabilised by a surfactant, lipid and/or polymer coating [3]. Due to the compressibility of the gas core, MBs undergo volumetric oscillations when exposed to a US field, and the resulting acoustic scattering may be used to enhance the contrast between blood vessels and the surrounding tissue in US images [4]. The use of sufficiently high acoustic pressures can lead to MB fragmentation and the dispersion of their coating material [5]. As the MB coating can be loaded with drugs through the addition of single therapeutic molecules, drug-loaded liposomes or other nanoparticles, the ability to non-invasively trigger the release of therapeutics using US makes MBs an attractive drug delivery

platform [6–8]. Additionally, US targeted MB destruction (UTMD) has been associated with increased payload distribution [9] and sonoporation [10] in tissue. Recent reviews of UTMD have summarized the use of this method for the delivery of chemotherapies [11,12], genes and thrombolytic drugs [13].

Several complementary targeting techniques have been developed to increase treatment localisation and so reduce potential side effects resulting from systemic administration. For example, MBs have been functionalised by attachment of antibodies enabling their binding to target tissues [14]. The short half-life of MBs (< 5 min in circulation) has presented a challenge for this method, and so acoustic radiation force has been investigated as a way to concentrate MBs and increase their binding to target sites [14,15]. Another approach has been to incorporate magnetic material into MBs and accumulate them in a target region using an external magnetic field [16]. This method was used in a recent study by the authors in which magnetically responsive

\* Corresponding authors.

E-mail address: [eleanor.stride@eng.ox.ac.uk](mailto:eleanor.stride@eng.ox.ac.uk) (E. Stride).

<sup>1</sup> Joint first authors.

<https://doi.org/10.1016/j.jconrel.2019.11.013>

Received 6 February 2019; Received in revised form 10 November 2019; Accepted 12 November 2019

Available online 13 November 2019

0168-3659/© 2019 The Authors. Published by Elsevier B.V. This is an open access article under the CC BY license (<http://creativecommons.org/licenses/by/4.0/>).

oxygen MBs (MgO<sub>2</sub>MBs) were used to deliver a combination of an antimetabolite drug (5-fluorouracil) and sonodynamic therapy (SDT) to pancreatic tumours [17]. While the combination of magnetic and US fields demonstrated an improved tumour growth delay and increased apoptotic cell signalling compared to the treatment with US only, the simultaneous application and alignment of magnetic and US fields produced by separate devices represented a significant practical challenge *in vivo*. This problem is particularly acute in small animal models due to space constraints and may greatly limit the potential synergistic benefits of magnetic-acoustic targeting. In the present study, this was addressed by using a prototype probe enabling co-aligned US and magnetic fields to be applied simultaneously [18]. The aim of the experiments described in the next section was to determine the effect upon drug delivery first *in vitro* in a tissue mimicking phantom and subsequently investigate the effect on treatment efficacy *in vivo* in a murine pancreatic cancer model.

## 2. Materials and methods

This section details the materials and suppliers used, followed by a description of the chemo/sonodynamic therapy complex used in all of the experiments and its *in vitro* evaluation with cultured cancer cells. The formulation and characterisation of drug-loaded, oxygen-filled, magnetically functionalised MBs are then presented and the devices for non-invasively providing magnetic and ultrasonic fields introduced. The section concludes with descriptions of the *in vitro* and *in vivo* experiments undertaken to determine the delivery potential of the drug loaded bubbles under different combinations of magnetic and ultrasound fields.

### 2.1. Reagents, equipment and software

Biotinylated Rose Bengal (RB) (compound 9) was prepared as described in [19]. Reagents used for the preparation of the chemo-sonodynamic drug complex combining the sonosensitiser Rose Bengal (RB) and antimetabolite drug gemcitabine (Gem) (compound 8) were purchased from Sigma Aldrich (Gillingham, Dorset, UK) at the highest grade available with the exception of biotin, di(N-succinimidyl) carbonate and 2-aminoethanol which were purchased from Tokyo Chemical Industry UK Ltd. NMR spectra were obtained on a Varian 500 MHz instrument (Palo Alto, CA, USA) at 25.0 ± 1 °C and processed using Bruker software (Billerica, MA, USA). Mass spectra were obtained on a Finnigan LCQMS instrument (San Jose, CA, USA).

The MBs were produced from a lipid mixture of 1,2-dibehenoyl-sn-glycero-3-phosphocholine (DBPC), 1,2-distearoyl-sn-glycero-3-phosphoethanolamine-N-[methoxy(polyethylene glycol)-2000] (DSPE-PEG2000) and DSPE-PEG2000-biotin from Avanti Polar Lipids (Alabaster, Alabama, USA). All reagents and equipment used for magnetic oxygen MB production were as previously described in [17] with the exception of the superparamagnetic iron oxide nanoparticles (IONPs) and therapeutic agent (*i.e.* 8). The IONPs (50 nm hydrodynamic diameter) were custom-conjugated by Ocean NanoTech (San Diego, CA, USA).

The design and calibration of the magnetic-acoustic device (MAD) having co-aligned acoustic and magnetic fields is described in [18]. The paraffin wax and US gel used during MAD testing were obtained from FullMoons Cauldron (Berkshire, UK) and Ana Wiz Ltd. (Anagel, Surrey, UK), respectively. UltraPure low melting point agarose was purchased from Thermo Fischer Scientific, (Paisley, UK) and the syringe pump was an AL-1000 from World Precision Instruments (Sarasota, FL, USA). Ultrasound drive signals were provided by a waveform generator (33500B, Keysight, Santa Rosa, CA, USA) and passed to a power amplifier (1040 L, E&I Ltd., Rochester, NY, USA). All ultrasound data sets were processed using MATLAB (Mathworks, Natick, MA, USA). Passive cavitation detection (PCD) was enabled by a single element focused transducer (7.5 MHz center frequency, 12.7 mm diameter, 75 mm focal

distance, Olympus NDT, Essex, UK). Signals were passed to a single stage preamplifier (SR455A, Stanford Research Systems, Sunnyvale, CA, USA) before streaming to computer disk using a two-channel digitizer (HS-3, TiePie Engineering, Sneek, Netherlands). Additional description of the methods used to acquire and analyse the PCD data are provided in the subsequent sections and summarized in the supporting information (section 5).

MBs were ruptured using an US bath (Eumax, UD150SH-6 L, 40 kHz, 150 W) prior to determining drug loading using a FLUOstar Omega multi-purpose plate reader from BMG Labtech (Aylesbury, Bucks, UK). The iron loading on MBs was determined by inductively coupled plasma - optical emission spectroscopy (ICP-OES) using an Optima 8000 instrument from Perkin Elmer (Seer Green, UK). Singlet oxygen sensor green (SOSG) was purchased from Thermo Fisher Scientific (Paisley, UK).

### 2.2. Preparation of chemo/sonodynamic therapy complex (biotin-RB-gem)

In our previous work, we investigated the combination of 5-fluorouracil (chemotherapy) and Rose-Bengal (sonodynamic therapy). As gemcitabine has been reported as the antimetabolite therapy of choice for pancreatic cancer, superseding treatments with 5-fluorouracil [20], recent work by the authors has also presented MBs loaded separately with gemcitabine and Rose Bengal [21] and this was the combination selected for the present study.

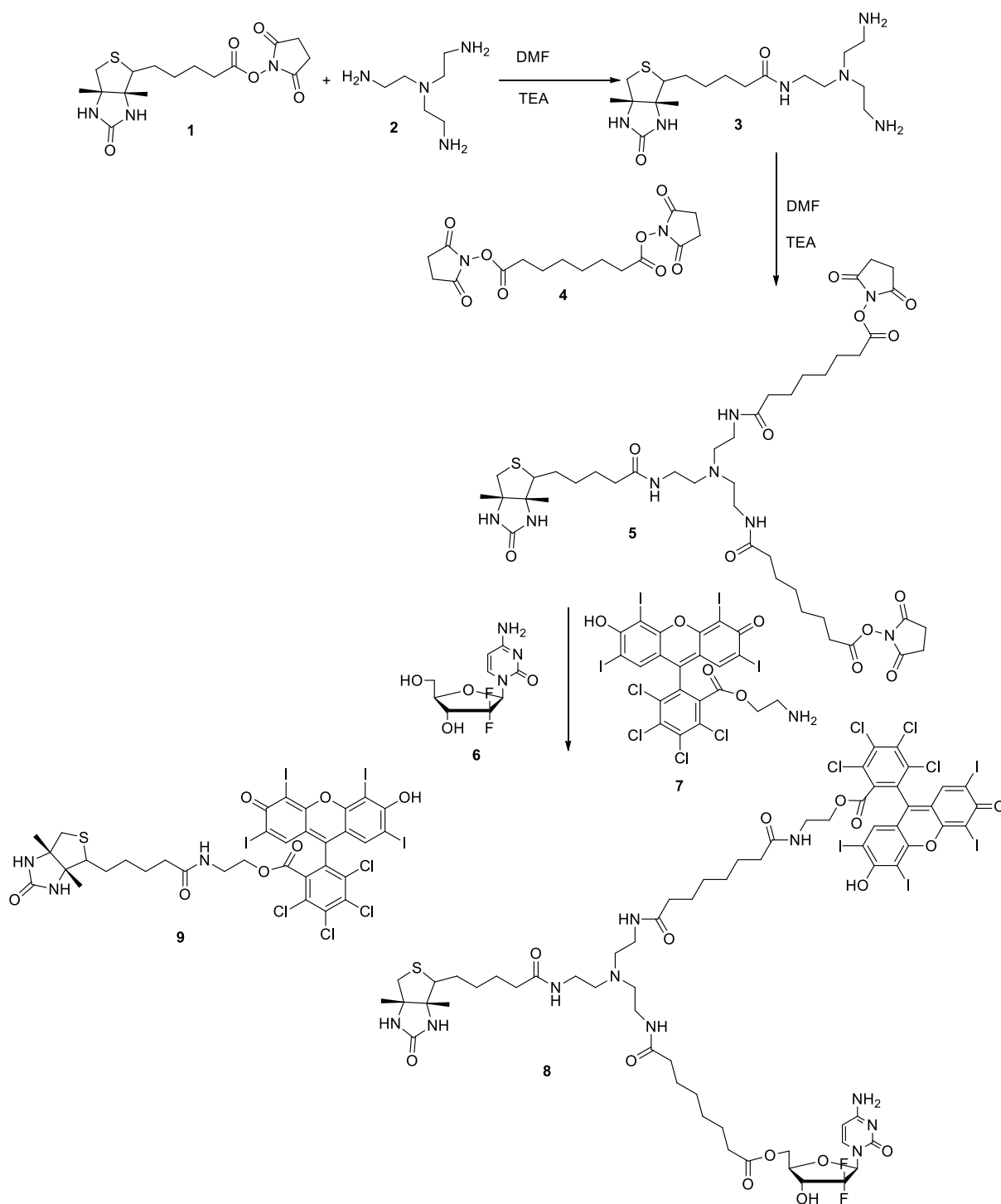
To enable the loading of both the RB and Gem on the MB surface, a novel therapeutic was formulated with a single biotin anchor connected to both drugs. The methods used to prepare this complex are described in this section following Scheme 1.

#### 2.2.1. Synthesis of N-(2-(bis(2-aminoethyl)amino)ethyl)-5-(2-oxohexahydro-1H-thieno[3,4-d]imidazol-4-yl)pentanamide (3)

To a stirred solution of tris(2-aminoethyl)amine (2) (0.22 g, 1.5 mmol) and trimethylamine (TEA) (catalytic amount) in anhydrous dimethylformamide (DMF) (5 mL), Biotin-NHS (1) (0.5 g, 1.5 mmol) was added and the reaction mixture was stirred at 0 °C under a nitrogen atmosphere for 30 min. The solvent was removed under reduced pressure and the residue was triturated with diethyl ether. The crude product was purified by column chromatography on basic (TEA) silica gel (methanol: dichloromethane 1:9 to 3:7) to give 3 (0.33 g, 61% yield) as a white semi solid. <sup>1</sup>H NMR (DMSO-*d*<sub>6</sub>): δ 7.94 (brs, 1H, NH), 6.42 (brs, 1H, NH), 6.35 (brs, 1H, NH), 4.49 (brs, 4H, NH<sub>2</sub> X 2), 4.29 (s, 1H, CH), 4.12 (s, 1H, CH), 3.07–3.02 (m, 6H, CH<sub>2</sub> X 3), 2.88–2.82 (m, 1H, CH), 2.44–2.06 (m, 10H, CH<sub>2</sub> X 5), 1.59–1.48 (m, 4H, CH<sub>2</sub> X 2), 1.47–1.29 (m, 2H, CH<sub>2</sub>). ESI-MS: calculated for C<sub>16</sub>H<sub>32</sub>N<sub>6</sub>O<sub>2</sub>S, 372.23; found 373.31 (M + H).

#### 2.2.2. Synthesis of bis(2,5-dioxopyrrolidin-1-yl) 8,8'-((((2-(5-(2-oxohexahydro-1H-thieno[3,4-d]imidazol-4-yl)pentanamido)ethyl)azanediyl)bis(ethane-2,1-diyl))bis(azanediyl))bis(8-oxooctanoate) (5)

To a stirred solution of compound 3 (0.5 g, 1.3 mmol) and TEA (catalytic amount) in 10 mL anhydrous DMF was added disuccinimidyl suberate (4, 1 g, 2.7 mmol) and the reaction mixture stirred at room temperature for 6 h under a nitrogen atmosphere. After completion of the reaction, excess diethyl ether (200 mL) was added to the reaction mixture. The white precipitate thus obtained was filtered and washed 3 times with diethyl ether (50 mL × 3). The crude product was purified by column chromatography on basic (TEA) silica gel (methanol: chloroform 2:8 to 5:5 v/v) to give 5 (0.83 g, 71% yield) as low melting white solid. <sup>1</sup>H NMR (DMSO-*d*<sub>6</sub>): δ 7.94 (brs, 2H, NH X 2), 7.67 (brs, 1H, NH), 6.41 (brs, 1H, NH), 6.34 (brs, 1H, NH), 4.29 (s, 1H, CH), 4.12 (s, 1H, CH), 3.06–3.04 (m, 3H, CH and CH<sub>2</sub>), 2.88–2.72 (m, 6H, CH<sub>2</sub> X 3), 2.71–2.63 (m, 8H, CH<sub>2</sub> X 4), 2.45–2.34 (m, 6H, CH<sub>2</sub> X 3), 2.20–2.06 (m, 10H, CH<sub>2</sub> X 5), 1.60–1.21 (m, 22H, CH<sub>2</sub> X 11). <sup>13</sup>C NMR (DMSO-*d*<sub>6</sub>): 172.5 (C=O), 170.7 (C=O), 163.1 (C=O), 162.7 (C=O), 61.4 (CH), 59.6 (CH), 55.8 (CH<sub>2</sub>), 53.9 (NCH<sub>2</sub>), 39.9 (CH<sub>2</sub>), 39.8 (CH<sub>2</sub>), 39.6 (CH<sub>2</sub>),



**Scheme 1.** Synthetic scheme for the production of biotin-RB-Gem (8) and biotin-RB (9).

37.3(CH<sub>2</sub>), 36.2(CH<sub>2</sub>), 35.6(CH<sub>2</sub>), 31.2 (CH<sub>2</sub>), 28.7(CH<sub>2</sub>), 28.5(CH<sub>2</sub>), 25.8(CH<sub>2</sub>), 25.7(CH<sub>2</sub>), 25.6(CH<sub>2</sub>). ESI-MS: calculated for C<sub>40</sub>H<sub>62</sub>N<sub>8</sub>O<sub>12</sub>S, 878.4; found 901.3 (M + Na salt).

**2.2.3. Synthesis of ((2R,3R,5R)-5-(4-amino-2-oxopyrimidin-1(2H)-yl)-4,4-difluoro-3-hydroxytetrahydrofuran-2-yl)methyl 4,11,19-trioxo-15-(2-(5-(2-oxohexahydro-1H-thieno[3,4-d]imidazol-4-yl)pentanamido)ethyl)-1-((2,3,4,5-tetrachloro-6-(6-hydroxy-2,4,5,7-tetraiodo-3-oxo-3H-xanthen-9-yl)benzoyl)oxy)-3,12,15,18-tetraazahexacosan-26-oate (8)**

To a stirred solution of 5 (0.4 g, 0.45 mmol) in anhydrous DMF (5 mL) was added gemcitabine hydrochloride (6, 0.136 g, 0.45 mmol)

and TEA (0.5 mL) and the reaction was stirred at 22 °C for 24 h under a nitrogen atmosphere. After completion of the reaction, Rose Bengal amine (7) (prepared separately according to [22]), (0.43 g, 0.45 mmol) in anhydrous DMF (5 mL) and TEA (0.5 mL) were added to the reaction mixture and continued to stir for 24 h. Once the reaction was complete, excess diethyl ether (200 mL) was added to the solution and stirred for 30 min. The pink red precipitate thus obtained was triturated with diethyl ether (100 mL), ethyl acetate (100 mL), acetone-water mixture (10%, v/v, 100 mL) and finally with ethyl acetate-hexane mixture (50%, v/v, 100 mL) respectively to afford a pink powder of compound 8 (0.26 g, 30% yield). <sup>1</sup>H NMR (DMSO-*d*<sub>6</sub>), Fig. S1: δ 7.95 (brs, 2H, NH<sub>2</sub>),

7.69 (s, 1H, CH, aromatic proton), 7.68 (s, 1H, CH, aromatic proton), 7.37(s, 1H, CH), 7.32 (brs, 4H, NH X 4), 6.89 (s, 1H, CH), 6.42 (brs, 1H, NH), 6.35 (brs, 1H, NH), 6.22 (d,  $J = 5.5$  Hz, 1H, CH), 6.13 (brs, 1H, NH), 5.78–5.77 (m, 1H, CH), 5.19 (s, 1H, CH X 2), 4.9 (brs, 1H, OH), 4.30 (s, 2H,  $-\text{OCH}_2$ ), 4.13 (s, 2H,  $-\text{OCH}_2$ ), 3.79–3.60 (m, 3H, CH,  $\text{CH}_2$ ), 3.39–3.32 (m, 2H,  $\text{CH}_2$ ), 3.07 (brs, 6H,  $\text{N}-\text{NHCH}_2$  X 3), 2.94–2.84 (m, 6H,  $\text{NCH}_2$  X 3), 2.81 (brs, 1H, OH), 2.45–2.46 (m, 3H, CH,  $\text{CH}_2$ ), 2.17–2.06 (m, 10H,  $\text{CH}_2$  X 5), 1.60–1.10 (m, 22H,  $\text{CH}_2$  X 11).  $^{13}\text{C}$  NMR ( $\text{DMSO}-d_6$ ), (Fig. S2) 171.8 (C=O, C), 165.98 (C=O), 163.2 (C=O), 162.7 (C=O), 159.3 (CH), 155.0 (C=O), 150.5 (C), 145.8 (C), 141.2 (CH), 131.0 (C), 128.7 (C), 123.5 (C), 116.2 (C), 95.0 (CH), 80.9 (C), 69.3 (CH), 61.5 (C), 59.6 ( $\text{CH}_2$ ), 59.4 (CH), 55.8 (CH), 51.7 ( $\text{CH}_2$ ), 45.8 ( $\text{CH}_2$ ), 40.2 ( $\text{CH}_2$ ), 37.3 ( $\text{CH}_2$ ), 37.05 ( $\text{CH}_2$ ), 36.2 ( $\text{CH}_2$ ), 35.5 ( $\text{CH}_2$ ), 31.0 ( $\text{CH}_2$ ), 28.7 ( $\text{CH}_2$ ), 28.5 ( $\text{CH}_2$ ), 28.2 ( $\text{CH}_2$ ), 25.6 ( $\text{CH}_2$ ). ESI-MS, (Fig. S3): calculated for  $\text{C}_{63}\text{H}_{72}\text{Cl}_4\text{F}_{14}\text{N}_{10}\text{O}_{15}\text{S}$ , 1925.98; found 1925.90 (M – H).

### 2.3. *In vitro* treatment of BxPC-3 and Mia-PaCa-2 cells with biotin-RB-gem and gemcitabine

The human primary pancreatic adenocarcinoma cell line BxPC-3 was maintained in RPMI 1640 medium which was supplemented with 100 U/mL penicillin, 100 mg/mL streptomycin, and 10% fetal bovine serum (FBS) in a humidified 5%  $\text{CO}_2$  atmosphere at 37 °C. The Mia-PaCa-2 cell line was maintained using Dulbecco's Modified Eagle's Medium (DMEM) containing 1 g/L glucose and supplemented with 100 U/mL penicillin, 100 mg/mL streptomycin, and 10% fetal bovine serum (FBS) in a humidified 5%  $\text{CO}_2$  atmosphere at 37 °C. These cells were seeded into 96-well plates at a density of 5000 cells per well. The plates were then incubated for 24 h followed by the addition of 100  $\mu\text{L}$  of media spiked with Gem or **8** at concentrations ranging from 0.001–1000  $\mu\text{M}$ . The cells were then further incubated for 48 h before the cell viability was determined by an MTT assay.

### 2.4. Preparation of drug-loaded magnetic MBs

Avidin functionalised magnetically responsive MBs (MagMBs) were prepared through the sonication of a lipid mixture containing DBPC:DSPE-PEG2000:DSPE-PEG2000-biotin at a ratio of (82:9:9) as previously described in [17]. However, in the current work, 1,2-dibehenoyl-sn-glycero-3-phosphocholine coated IONPs were used (3.75 mg iron) instead of FluidMAG-Lipid nanoparticles, in order to use the same lipid as the one composing the MB coating. Compound **8** or **9** (1 mL, 5.2 mM in PBS with 0.5% (v/v) DMSO) was loaded onto the MagMBs following the method reported in [17]. All MBs evaluated in this manuscript were washed three times by centrifugation to remove excess material from the suspension. *In vitro*, MagMB characterisation was completed using **9** to prevent wastage of the more difficult to synthesise **8**. Drug-loaded MagMBs were kept in reduced light conditions and on ice prior to use and are referred to as  $\text{MgO}_2\text{MB-RB-Gem}$  (Fig. 1) or  $\text{MgO}_2\text{MB-RB}$  depending on which drug product was used. If the samples were not sparged with oxygen, they are referred to as  $\text{MagMB-RB-Gem}$  and  $\text{MagMB-RB}$ .

### 2.5. Characterisation of MB size and concentration

The MBs were characterised for their size and concentration following analysis of optical microscope images using a custom MATLAB script [23]. For this, a 10  $\mu\text{L}$  aliquot of a diluted (1:20 v/v) sample in PBS was loaded onto a haemocytometer and imaged 30 times using an optical microscope fitted with a 40 $\times$  objective, leading to approximately 1800 MBs examined per MB batch.

### 2.6. Characterisation of MB drug loading

The drug loading of MBs was investigated for both **8** and **9** using

UV–Vis spectroscopy. As the ratio of RB to Gem in each molecule of **8** is 1:1, the concentration of both Gem and RB attached to  $\text{MgO}_2\text{MB-RB-Gem}$  can be determined from the RB absorbance at 559 nm, using a previously constructed calibration graph. Similarly, for **9**, the RB concentration of  $\text{MgO}_2\text{MB-RB}$  was determined based on the RB absorbance at 559 nm. For each MB batch prepared, a 50  $\mu\text{L}$  sample of MBs was sonicated (40 kHz ultrasound bath) for 5 s before diluting it (1:100 v/v) and recording the absorbance at 559 nm using a plate-reader.

### 2.7. Characterisation of MB iron loading

As DBPC-IONPs were incorporated within the MB coating, the functionalisation of MBs with drug products on its outer surface is unlikely to affect the iron loading of the MBs. The iron content of MBs was therefore measured without the addition of drugs to prevent wastage of synthesised ligands, and was determined by ICP-OES measurements of samples diluted in 2% nitric acid at a wavelength of 238 nm.

### 2.8. Production of singlet oxygen from $\text{MgO}_2\text{MB-RB}$ exposed to US

The production of singlet oxygen ( $^1\text{O}_2$ ) from activated RB exposed to US was determined using SOSG. A sample of 9 mL degassed PBS,  $\pm 5 \times 10^7$  MB/mL,  $\pm 541$   $\mu\text{M}$  biotin-RB, and 1.25  $\mu\text{M}$  SOSG was exposed to 1.17 MHz, 0.70 MPa peak negative pressure, 30% duty cycle (DC), 100 Hz pulse repetition frequency (PRF) US for 3.5 min. Sample exposure was undertaken using a custom-made tank with the built-in transducer driven at 1.17 MHz. The sample was injected into a holder placed in the pre-focal region of the transducer to ensure a uniform pressure field at the top of the sample chamber. The fluorescence intensity of SOSG (Ex: 490 nm / Em: 520 nm) was measured for each sample with and without US exposure. To minimize the scattering from MBs in the sample without US exposure, increased hydrostatic pressure was applied to the sample using a sealed syringe to destroy the bubbles prior to fluorescence measurement. The generation of  $^1\text{O}_2$  was then calculated as a percent change in SOSG fluorescence intensity at 520 nm for a sample exposed to US compared to a control sample for each experimental run. In addition to measuring  $^1\text{O}_2$  generation, the characterisation of MB acoustic emissions during US exposure were recorded using PCD focused on the top of the sample chamber. A 2 MHz analog high-pass filter was used to remove the drive frequency from the recorded signal before pre-amplification, digitization, and storage onto a computer drive. The power spectral density was calculated for each PCD signal acquisition. These results were used to quantify cavitation activity during each experiment (3.5 min exposure) by determining the cumulative energy at ultraharmonic frequencies ( $f_0^*(n + 0.5)$ ), with  $f_0 = 1.17$  MHz and  $n = 2, 3, \dots, 09$ , which are indicative of nonlinear bubble oscillations.

### 2.9. Magnetic-acoustic-device (MAD) and control device

The MAD was designed as described by Barnsley et al. and assembled as shown in Fig. 2 [18]. Briefly, the magnetic body consisted of N52 grade NdFeB permanent magnet material whose geometry was optimized to have a maximum magnetic field of 0.2 T at a distance of 10 mm from the body's leading edge. An integrated ultrasonic element with a focal distance also of 10 mm provided a pressure field that spatially overlapped with the magnetic field peak, with sufficient amplitude to cause inertial cavitation of MBs used in this study. An aluminium-bodied copy of the MAD (hereafter referred to as "aMAD") was produced to provide an US-only control for *in vitro* and *in vivo* experimentation.

In order to span the gap between the US element and the delivery site of interest in the present work, a coupling cone (Fig. 2) was cast from paraffin wax and secured with US gel. The cone material was



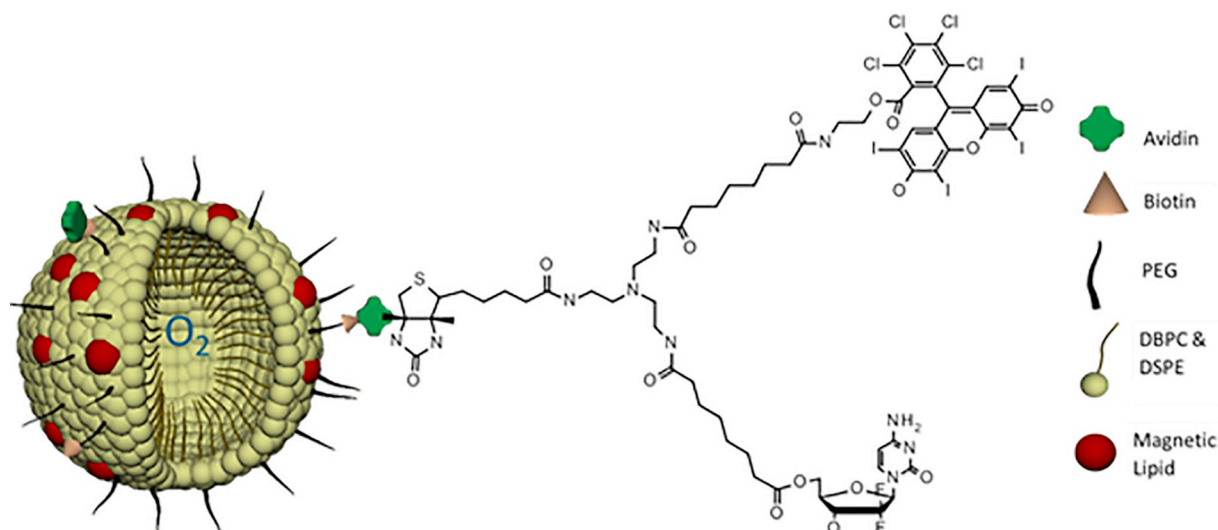


**Fig. 1.** Schematic representation of the MagO<sub>2</sub>MB-RB-Gem conjugate.

chosen for its ease of casting and minimal transmission loss in the 1 MHz frequency range as determined by through-transmission measurements. Since the acoustic boundary conditions for this configuration were different from those used in the initial characterisation [18], both the MAD and the aluminium copy were recalibrated (Fig. S4).

### 2.10. Drug delivery comparison in agar between devices

Drug delivery was quantified *in vitro* by flowing MagO<sub>2</sub>MB-RB through a tissue mimicking agar phantom (Fig. 3). The phantom body was formed within a Delrin frame filled with 1.25% agar gel. The cured agar phantom was 7 mm thick and covered in clear and acoustically transparent Mylar films on each side. Each phantom contained at least one straight channel of 1.2 mm diameter, with fittings on the frame for connection to a syringe pump and drain tubing. During testing, the phantom was partially immersed in a water bath heated to  $36 \pm 1^\circ\text{C}$ , with the upper phantom surface in air so that acoustic boundary conditions would be similar to those in the *in vivo* experiments. The phantom assembly was free of ferrous metal parts in order to minimize the likelihood of secondary magnetic fields influencing the results.

For acoustic treatments (MAD or aMAD), the device was held in place with a lab clamp, and the cone tip was coupled to the phantom

face with water. Acoustic drive pulses (3000 cycles of 1.17 MHz, 30% duty cycle) were provided so that the peak negative pressure 10 mm in front of the device would be 0.7 MPa.

Ultrasonic emissions from the channel were recorded using a single PCD. Signal conditioning and post-processing procedures were performed using the same procedures and instrumentation as in Section 2.8. Initial positioning of the agar flow channel and the acoustic instrumentation was guided by a crosshair laser to ensure proper alignment. Data were collected for six groups as indicated in [Table 1](#), with three separate phantoms tested per group. The MAD was used for: (1) its co-aligned magnetic and acoustic fields (group: “MAD” and shown in [Fig. 3A](#), (2) its magnetic field only (US off) (group: “Mag”), and (3) its magnetic field (MAD US off) with the acoustic field of the (aMAD) to study the non-coaligned fields (group: “US + Mag”), and shown in [Fig. 3B](#). The aMAD was also used on its own for the US only control (group: “US”).

For all treatment groups, 100  $\mu$ L of MagMB-RB ([MB] =  $(1.74 \pm 0.62) \times 10^8$  MB/mL, [RB] =  $506 \pm 53$   $\mu$ M) were injected at a flow rate of 0.2 mL/min. US was applied for 3.5 min, after which the treated channel was rinsed with 1 mL deionised water. The agar channel was immediately cut out (0.7 mL volume) and reserved for analysis after the experiment. After all groups were completed in a

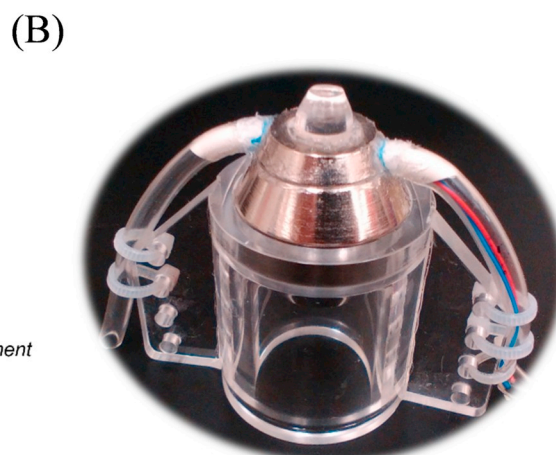
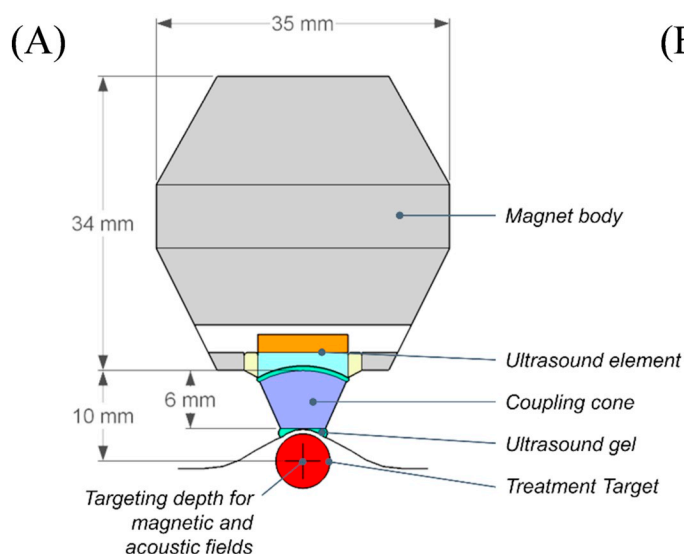


**Fig. 2.** (A) MAD configuration illustration and (B) photograph as tested, with Perspex holder.

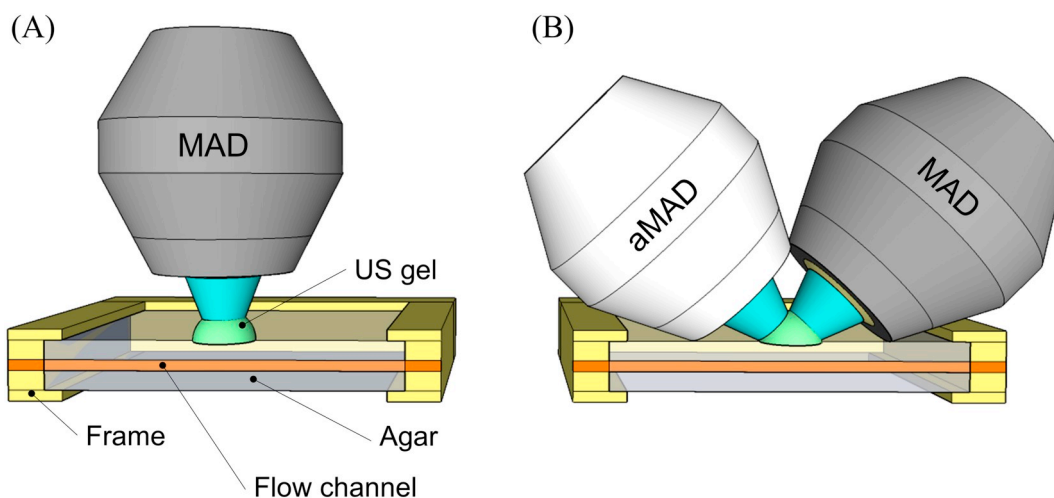


**Fig. 3.** *In vitro* flow phantom set-up for (A) the MAD with co-aligned fields compared to (B) the separate but simultaneous application of magnetic (MAD with US element turned off) and US (aMAD) fields. Phantom is shown cutaway to visualize the 1.2 mm diameter channel through which MMBs were flown. The underlying water bath is not shown.

**Table 1**

*In vitro* drug delivery experiment groups.

Group Name	Water	MagMB-RB <sup>a</sup>	US <sup>b</sup>	Magnet <sup>c</sup>
Untreated	X			
MB		X		
US		X	X (aMAD)	
Mag		X		X (MAD)
US + Mag		X	X (aMAD)	X (MAD)
MAD		X	X (MAD)	X (MAD)

<sup>a</sup> MagMB-RB: MB =  $(1.7 \pm 0.6) \times 10^8$  MB/mL and [RB] =  $500 \pm 50$   $\mu$ M.

<sup>b</sup> US: 1.17 MHz, 30% duty cycle, peak negative pressure 0.7 MPa, 3.5 min.

<sup>c</sup> Magnet: 0.2 T at 10 mm.

single test day, the reserved cut out agar channels were melted, sampled onto a pre-heated 96-well plate and left to equilibrate at 45 °C for 15 min. Absorbance spectra were acquired at that temperature using a plate reader to measure the amount of RB delivered in the agar volume. Spectra were normalised to no-treatment controls and the samples' absorption intensities at 559 nm were compared to a standard curve for biotin-RB in melted 1.25% agar at 45 °C ( $R^2 = 0.9991$ ).

### 2.11. Treatment of xenograft ectopic BxPC-3 tumours in SCID mice

All animals employed in this study were treated in accordance with the licenced procedures under the UK Animals (Scientific Procedures) Act, 1986. BxPC-3 cells ( $1 \times 10^6$ ) in 50  $\mu$ L Matrigel + 50  $\mu$ L media (RPMI 1640) were subcutaneously implanted into the rear dorsum of 6–8 week year old SCID (C-B-17/IcrHan<sup>®</sup>Hsd-Prkdcscid) mice. Tumours started to form approximately two weeks after cell implantation, and once they became palpable, their sizes were measured using the Peira TM900 tumour measuring device (Beerse, Belgium). The TM900 platform software includes a measurement function enabling the visualisation of the tumour topography, allowing tumour dimensions (weight, length and height) to be automatically measured. When the tumours reached an average of  $113 \pm 13.42$  mm<sup>3</sup> the animals were distributed randomly into four groups (Table 2) using the randomization function in the TM900 platform.

Subjects were anaesthetized with intraperitoneal injections of Hypnorm / Hypnovel. A 100  $\mu$ L mixture of PBS with MagO<sub>2</sub>MB-RB-Gem ([MB] =  $(1.25 \pm 0.41) \times 10^9$  MB/mL, [biotin-RB-Gem] =  $521 \pm 80$   $\mu$ M) was administered by tail vein injection to the subjects receiving treatment. The drive instrumentation and settings were the same as those used for the *in vitro* drug delivery experiments described in Section 2.10. The cone of

**Table 2**

*In vivo* drug delivery experiment groups.

Group name	No treatment	MagO <sub>2</sub> MB-RB-Gem <sup>a</sup>	US <sup>b</sup>	Magnet <sup>c</sup>
Untreated	X			
MB		X		
US + Mag		X	X (aMAD)	X (MAD)
MAD		X	X (MAD)	X (MAD)

<sup>a</sup> MagO<sub>2</sub>MB-RB-Gem: [MB] =  $(1.3 \pm 0.4) \times 10^9$  MB/mL, [biotin-RB-Gem] =  $520 \pm 80$   $\mu$ M.

<sup>b</sup> US: 1.17 MHz, 30% duty cycle, peak negative pressure 0.7 MPa, 3.5 min.

<sup>c</sup> Magnet: 0.2 T at 10 mm.

the MAD (or aMAD) was coupled to the skin of the subject using US gel. In order to minimize acoustic field uncertainties and tissue damage risk, the subjects were treated lying prone over a mat of US absorbing material (Aptflex F28, Precision Acoustics, Dorset, UK). To improve free transmission of sound into the absorber, the abdominal hair was removed from the subjects, and their skin coupled to the mat with US gel. Using these methods, treatments were performed on days 0, 2 and 4. Subject weight and tumour size were monitored for 28 days after the first treatment. Previous data obtained from ectopic BxPC3 tumours treated with gemcitabine (120 mg/kg; IP; 2 x week) have been included in the results section for reference.

### 2.12. Statistics

With the exception of the tumour volumes in the *in vivo* experiments, results are expressed as the mean value  $\pm$  one standard deviation. Tumour volume data are reported as mean  $\pm$  standard error on account of the uncertainty in the mean tumour volume measurement. Statistical significance and comparisons were established using an unpaired *t*-test when evaluating two groups and a 1-way ANOVA followed by Tukey's *post hoc* test when comparing more than two groups using Microsoft Excel 365.

## 3. Results and discussion

### 3.1. Synthesis of biotin-RB-gem (8) and its efficacy in pancreatic cancer cells

To enable both the SDT sensitizer RB and antimetabolite Gem to be conjugated to the MB surface, MBs were surface functionalised with avidin and a tripodal ligand was designed to have a single biotin anchor

connected to both RB and Gem (**8**). To synthesise **8**, the N-hydroxysuccinimide ester of biotin (**1**) was first reacted with tris(2-aminoethyl)amine (**2**) in a 1:1 M reaction to encourage only one of the primary amines on **2** to form an amide bond with **1**. The resulting product **3**, was then reacted with disuccinimidyl suberate (**4**) in a 1:2 M ratio forming amide bonds with the remaining two primary amine residues of **3**, yielding compound **5** that also contained two pendant active esters. The active esters of **5** were reacted in turn with gemcitabine (**6**) and amine derivatised Rose Bengal (**7**), generating ester and amide linkages respectively with **5** to form target compound **8**. The structure of **8** was characterised using  $^1\text{H}$  and  $^{13}\text{C}$  NMR spectroscopy and positive electrospray mass spectroscopy (Figs. S1–S3). The mass spectrum reveals a base peak of 1925.9 Da corresponding to the exact mass of **8**. In addition,  $^1\text{H}$  NMR analysis of **8** showed the expected 1:2 integration ratio between each of the aromatic protons on the cytosine moiety of Gem (5.77 ppm and 7.37 ppm) and the two equivalent aromatic protons present on RB (7.68 ppm) as well as the characteristic urea protons of biotin at 6.38 ppm and 6.42 ppm.

Following the preparation and characterisation of compound **8**, the next step was to perform *in vitro* testing with pancreatic cancer cells, in order to ensure that derivatising Gem for incorporation within **8** did not impair its efficacy. BxPC-3 and MiaPaCa-2 cells were incubated with **8** at a range of concentrations from 0.001  $\mu\text{M}$  to 1.0 mM and cell viability determined 48 h later using the MTT assay. As a comparison, cells were also treated with the same concentrations of free Gem. The results are shown in Fig. 4 and reveal no significant difference in the median lethal dose ( $\text{LD}_{50}$ ) values for **8** ( $0.71 \pm 0.16 \mu\text{M}$  and  $0.74 \pm 0.19 \mu\text{M}$ ) or gemcitabine ( $362.30 \pm 0.12 \mu\text{M}$  and  $474.40 \pm 0.13 \mu\text{M}$ ) in BxPC-3 or Mia-PaCa-2 cells respectively. These results suggest that the ester bond connecting Gem in **8** is rapidly hydrolysed by endogenous esterase enzymes to liberate free Gem. These results also suggest no additional contribution to the cytotoxicity of **8** by RB in the absence of light or US stimulation. Furthermore, while it is important for cellular cleavage of Gem to enable its activation by deoxycytidine kinase mediated phosphorylation, rapid cleavage of RB from **8** is less important, as the mechanism of action for SDT does not require the sensitiser to bind to a receptor or be metabolised for reactive oxygen species to be generated.

### 3.2. MB characterisation

MagO<sub>2</sub>MBs were manufactured through the sonication of a mixture of phospholipids, surfactants and phospholipid-coated IONPs under PFB gas flow which resulted in a MB concentration of  $1.8 \pm 0.3 \times 10^9$  MB/mL and  $1.6 \pm 0.3 \mu\text{m}$  mean MB diameter. The removal of excess material through centrifugation significantly decreased the MB concentration to an average of  $7.5 \pm 4.0 \times 10^8$  MB/mL ( $p < .01$ ) and the

mean diameter to  $1.9 \pm 0.4 \mu\text{m}$  (Fig. 5). A comparison of the size distributions from before and after conjugation with **9** suggests that the loading and subsequent washing processes removes the smallest MBs (Fig. 5). However, the 1–8  $\mu\text{m}$  diameter MBs appear to be stable during this process and the mean hydrodynamic diameter of the population was not significantly affected by the washing procedure.

Detailed characterisation of the MB stability and their magnetic and acoustic properties prior to drug loading was reported in [24]. The iron content measured in the present study was 0.07 pg iron per MB after three centrifuge steps. This is higher than the previously reported values of 0.025 pg iron / MB [24] but was associated with manipulation variations in the resuspension of MBs during cleaning. This loading was calculated to equate to approximately 10% coverage of the MBs (supporting information) and their response to a magnetic field was confirmed visually (Fig. S5).

Analysis of the power of acoustic emissions over time from the MBs indicated that the surface addition of drugs on MBs significantly lengthened the time over which an increase in acoustic emissions was recorded compared to magnetic MBs without drug (Fig. S6). These results suggest that the surface functionalisation of MBs can provide a stabilising effect by dampening the oscillations of MBs. The drug concentration in the suspension after washing was  $480 \pm 100 \mu\text{M}$  or  $520 \pm 50 \mu\text{M}$  for **8** or **9** respectively.

The performance of oxygen-sparged lipid-based MBs to enhance sonodynamic therapy of hypoxic tumours was previously demonstrated by McEwan et al., showing *in vitro* that oxygen was released upon ultrasound exposure of diluted oxygen sparged MBs and *in vivo* that the expression of HIF1 $\alpha$  was significantly decreased in hypoxic tumours treated with oxygen MBs compared to perfluorobutane MBs [25].

### 3.3. In vitro activation and delivery

Using the US parameters indicated in Table 1, the results from the *in vitro* activation of RB using MagO<sub>2</sub>MBs and US are shown in Fig. 6. The generation of cytotoxic  $^1\text{O}_2$  was significantly enhanced when MagO<sub>2</sub>MB-RB in degassed PBS were exposed to US, compared to MagO<sub>2</sub>MBs or RB alone ( $p < .01$ ), thereby indicating the activation of the sensitiser RB through exposure to MBs and ultrasound. A similar trend was observed in the ultraharmonic energy of MB emissions recorded from the PCD, but the emissions from the two types of MB and RB alone were all significantly different ( $p < .01$ ). The increased cavitation activity of MagO<sub>2</sub>MB-RB compared to MagO<sub>2</sub>MBs could be explained by an enhanced stabilisation of MagO<sub>2</sub>MB-RB due to the surface functionalisation of the sensitiser that prevents bubble dissolution in the degassed medium [26]. As previously mentioned, this is further supported by the results in Fig. S6.

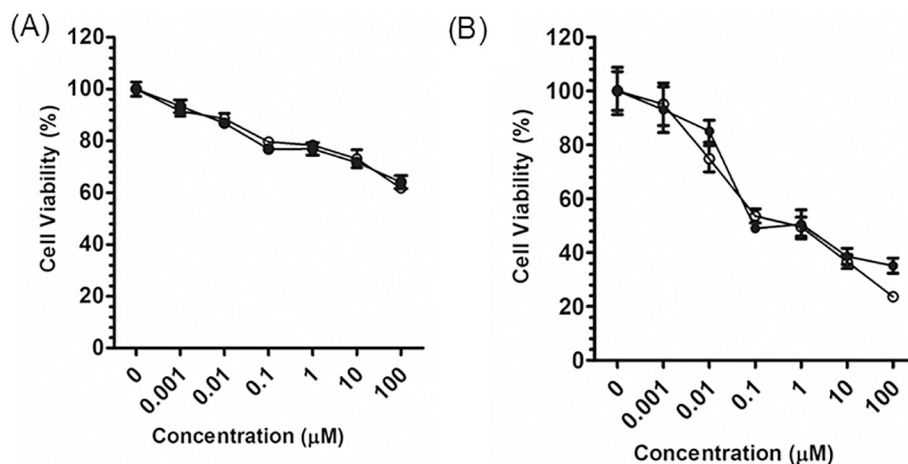
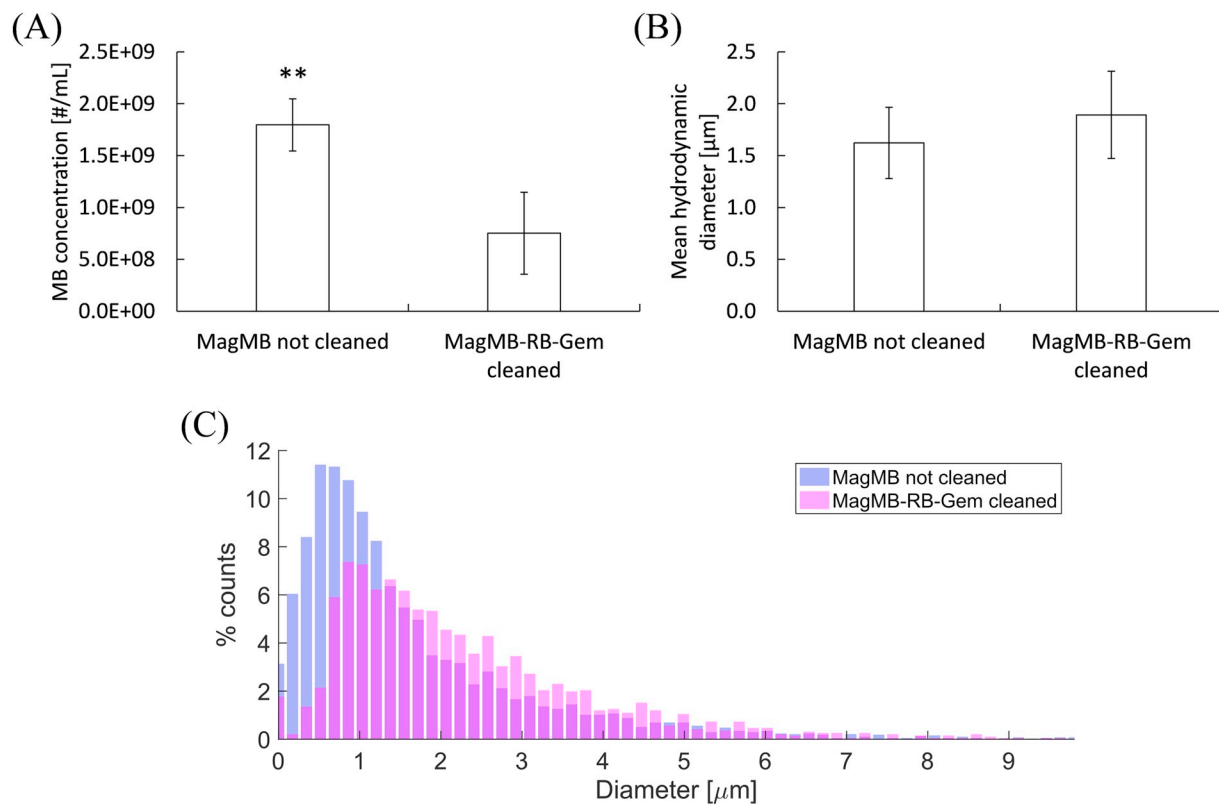


Fig. 4. MTT assay comparing the efficacy of biotin-RB-Gem (**8**) (open circles) and gemcitabine (filled circles) (A) BxPC-3 and (B) Mia-PaCa-2 cell lines.



**Fig. 5.** The effect of cleaning and drug conjugation on MB (A) concentration (\*\*  $p < .01$  calculated through an unpaired  $t$ -test with equal variance) and (B) mean hydrodynamic diameter; evaluated for  $n = 4$  batches per group. The concentration of MagMB-RB-Gem after washing was  $7.5 \pm 4.0 \times 10^8$  MB/mL and the mean diameter was  $1.9 \pm 0.4$  μm. (C) Example of size distribution of MagMBs before and after loading of biotin-RB-Gem obtained from analysis of 30 optical microscope images for each batch.

The performance of the MAD compared to the use of two separate devices and the contributions of US and of the magnetic field individually were assessed in an agar phantom containing a cylindrical flow channel (Fig. 3). The concentration of RB delivered was determined based on the absorbance of a set volume of agar gel surrounding a channel after flowing 100 μL of MagMB-RB through it while exposed to one of the device configurations. Fig. 7 shows the concentration of RB delivered for the different groups considered, and when US was used, the associated cavitation activity is provided. A significantly higher quantity of RB was delivered ( $p < .01$ ) using the MAD compared to all other groups; more specifically a 1.6 and 1.4-fold increase in RB was measured compared to the US only and US + Mag groups respectively. Moreover, a comparison between the MAD and US

only groups indicate a significant increase in delivery ( $p < .01$ ) from the addition of magnetic targeting, but the minimal enhancement observed for the US + Mag group compared to US highlights the difficulty in optimally aligning devices when two separate units are used. The delivery recorded for MagO<sub>2</sub>MB-RB alone (*i.e.* no magnet or US) could be associated with residual RB, potentially from lipid shell fragments, in the suspension diffusing across pores in the agar gel [27] and was found to be significant compared to the untreated group ( $p < .01$ ). Individually, US and Mag fields enhanced delivery to a similar degree, in agreement with previous results from Stride et al. [28].

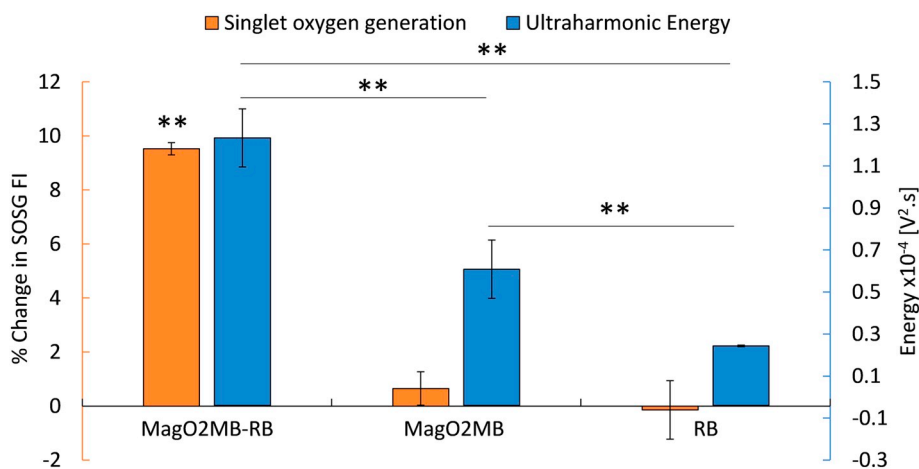


**Fig. 6.** Singlet oxygen production (orange,  $n = 3$ ) from RB activation after US exposure, with associated ultraharmonic emissions from MBs (blue) undergoing nonlinear oscillations. \*\* =  $p < .01$  determined through a 1-way ANOVA with Tukey's *post hoc* test. A sample was prepared with  $\pm 5 \times 10^7$  MB/mL,  $\pm 541$  μM biotin-RB, and 1.25 μM SOSG in degassed PBS. US parameters were 1.17 MHz, 0.7 MPa peak negative pressure, 30% duty cycle, 100 Hz pulse repetition frequency for 3.5 min. (For interpretation of the references to colour in this figure legend, the reader is referred to the web version of this article.)



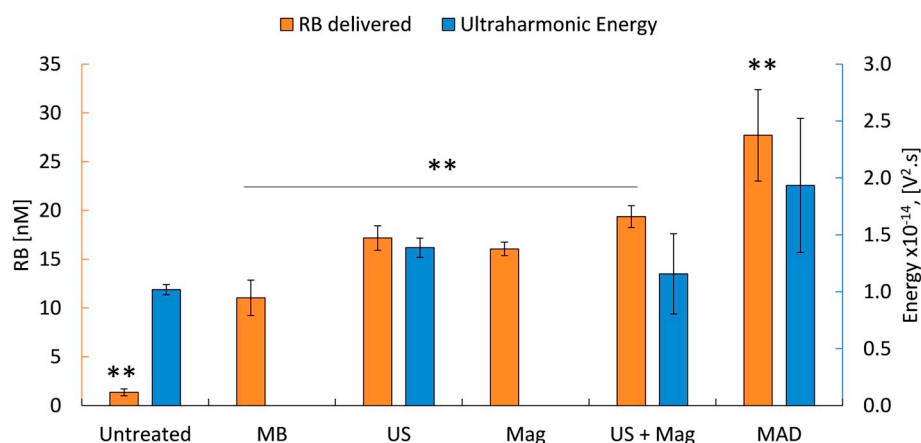


**Fig. 7.** RB drug delivery (orange,  $n = 3$ ) in a volume of 0.7 mL agar (1.25% w/w) with different ultrasound and magnetic device configurations as listed in Table 1. \*\* =  $p < .01$  determined through a 1-way ANOVA with Tukey's *post hoc* test. The corresponding ultraharmonic emissions of MBs (blue) are shown. For the treatment-receiving groups, 100  $\mu\text{L}$  of MagMB-RB ([MB] =  $1.74 \pm 0.62 \times 10^8$  MB/mL, [RB] =  $506 \pm 53 \mu\text{M}$ ) were administered and flown at 0.2 mL/min. When a magnet was used, a 0.2 T magnetic field from the MAD was applied at the US focus. When US was applied (MAD or aMAD), the parameters were: 1.17 MHz, 0.7 MPa peak negative pressure, 30% duty cycle (DC), 100 Hz PRF for 3.5 min. The ultraharmonic emissions plotted for the untreated group reflect the background noise recorded with water flowing in the agar channel. (For interpretation of the references to colour in this figure legend, the reader is referred to the web version of this article.)

### 3.4. In vivo results

To test the utility of the MAD as a platform for the delivery of combined magnetic and US fields *in vivo*, SCID mice were implanted with ectopic human pancreatic BxPC-3 tumours and randomly distributed into 4 groups for treatment as described in Table 2. The results in Fig. 8 indicate a 37% reduction in tumour volume relative to the pre-treatment volume days after the initial treatment for animals treated with MagO<sub>2</sub>MB-RB-Gem and the MAD, compared to a 9% reduction when combined magnetic and US fields were simultaneously delivered using separate probes (M + U). This difference was maintained for 4 days, and 12 days following the initial treatment, tumours treated with MagO<sub>2</sub>MB-RB-Gem and the MAD were still 9% smaller than their pre-treatment volume and 54% smaller than tumours treated with MagO<sub>2</sub>MB-RB-Gem and separate probes. Beyond day 12, all groups showed tumour growth. The MAD group showed the least, but there was no statistically significant difference from the separate probe group. This indicates that further investigation of the treatment schedule with larger groups is warranted.

The observed differences between treatments performed with the MAD and physically separate but simultaneous magnetic and ultrasonic field generating devices illustrate the importance of field alignment. When co-aligned as in the MAD, the tendency of bubbles to be pushed away from the US focus by radiation force is counteracted by the pulling force of the magnet. This effect, which helps maintain a population of bubbles in the US beam, is weaker and potentially becomes

detrimental to bubble availability in the US focus when the ultrasonic and magnetic fields are separated by a large angle, as with the separate device tests.

Taken together, these results demonstrate an improved therapeutic effect obtained from the co-aligned application of magnetic and acoustic fields using one device compared to the use of two separate devices. Additionally, the chemo-sonodynamic therapy delivered using the MAD provided a rapid, substantial and stable reduction in tumour volume, suggesting that this approach may be useful as a neoadjuvant treatment to downstage pancreatic tumours in advance of surgery. There is a large proportion of pancreatic cancer patients (~20%) presenting with borderline resectable lesions, and a reduction in tumour burden could make them eligible for surgical resection. As 5-year survival rates improve 5-fold when surgery is possible, effective neoadjuvant strategies that increase resection rates are the fastest way to improve survival in a disease that has witnessed only minor improvements over the past 40 years [29,30]. The approach outlined in this manuscript was not only effective at reducing tumour burden but was also well tolerated, as the animals remained healthy and exhibited no weight loss over the duration of the study (Fig. S10). Scaling of the MAD to human length scales is demonstrated in [18].

### 3.5. Limitations

Although the results shown in Figs. 8 and S10 are encouraging, there are several limitations of the work that need to be discussed. First,

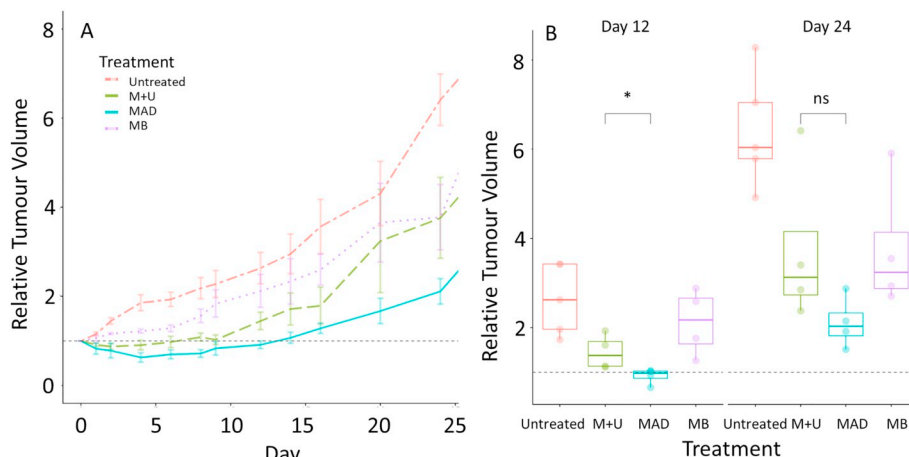


**Fig. 8.** *In vivo* results with (A) tumour growth over time relative to day 0. Treatments were given on days 0, 2, and 5. (B) Comparison of relative tumour volumes at days 12 and 24 (\*  $p < .05$  determined by an unpaired *t*-test,  $n = 5$  for untreated and  $n = 4$  for MAD, MB, and M + U).

the MAD used in this study was designed for small animal experiments but, as discussed in [18], a compromise had to be made between peak magnetic force and acoustic pressure at the focus. This will be overcome in future development of the device, which will also include treatment monitoring capability. Second, it was not possible with the equipment available to assess tumour vascularity prior to treatment. This is, however, likely to be an important predictor of therapeutic response as it determines the quantity of MBs entering the target volume. Whilst ultrasound and MBs are able to improve the distance to which therapeutic material is delivered from the nearest blood vessel, they cannot compensate entirely for poor perfusion. This then contributes to the variance in tumour volumes which was notably higher in the results for the groups without magnetic field (Fig. 8, S7, S9). Finally, residual RB and Gem potentially from MBshell fragments, suggested by the *in vitro* results, could also explain the decreased tumour size observed in subjects receiving MBs only, compared to no treatment. Further development of the therapeutic MBs will focus on product loading and cleaning protocols to minimize off-target accumulation and undesired side-effects.

#### 4. Conclusions

A novel therapeutic incorporating the antimetabolite Gemcitabine, the sensitiser Rose Bengal and the attachment ligand biotin was synthesised and enabled the simultaneous loading of both drugs onto oxygen-filled magnetic MBs. The co-aligned application of magnetic and ultrasound fields to the target region using the MAD produced an increase in drug deposition *in vitro* and tumour response *in vivo* compared to the application of both fields using two separate devices. These results indicate the importance of co-alignment of the magnetic and ultrasound fields and provide further supporting evidence for the potential use this approach to downstage pancreatic tumours in cancer patients with borderline resectable lesions, enabling them to undergo surgery.

#### Acknowledgements

The authors thank James Fisk and David Salisbury for their contribution to the design and construction of the *in vitro* US tanks, phantom holders and the aluminium device copy used in this work. Funding for the work was provided by the Engineering and Physical Sciences Research Council (EP/I021795/1 and EP/L024012/1) and the Institute of Engineering and Technology (AF Harvey Prize). EB thanks the Research Councils UK Digital Economy Programme for the support through grant EP/G036861/1 (Oxford Centre for Doctoral Training in Healthcare Innovation). MDG was supported by the National Institute of Health Research, Oxford Biomedical Research Centre. JFC thanks Norbrook Laboratories Ltd. for an endowed chair. KAL thanks the Department for the Economy in Northern Ireland for a PhD studentship. YS and SK thank Invest N.I. in Northern Ireland and the Pancreatic Cancer Research Fund respectively for postdoctoral fellowships.

#### Appendix A. Supplementary data

Supplementary data to this article can be found online at <https://doi.org/10.1016/j.jconrel.2019.11.013>. Raw data are available at <https://doi.org/10.5287/bodleian:ZBwQzkJaw>

#### References

- [1] G. Dimcevski, S. Kotopoulos, T. Bjånes, D. Hoem, J. Schjot, B.T. Gjertsen, M. Biermann, A. Molven, H. Sorbye, E. McCormack, M. Postema, O.H. Gilja, A human clinical trial using ultrasound and microbubbles to enhance gemcitabine treatment of inoperable pancreatic cancer, *J. Control. Release* (2016), <https://doi.org/10.1016/j.jconrel.2016.10.007>.
- [2] A. Carpentier, M. Canney, A. Vignot, V. Reina, K. Beccaria, C. Horodyckid, C. Karachi, D. Leclercq, C. Lafon, J.Y. Chapelon, L. Capelle, P. Cornu, M. Sanson,

- K. Hoang-Xuan, J.Y. Delattre, A. Idbaih, Clinical trial of blood-brain barrier disruption by pulsed ultrasound, *Sci. Transl. Med.* 8 (2016) 343re2, <https://doi.org/10.1126/scitranslmed.aaf6086>.
- [3] S.R. Sirsi, M.A. Borden, Microbubble compositions, properties and biomedical applications, *Bubble. Sci. Eng. Technol.* 1 (2009) 3–17, <https://doi.org/10.1179/175889709X446507>.
- [4] V.R. Stewart, P.S. Sidhu, New directions in ultrasound: microbubble contrast, *Br. J. Radiol.* 79 (2006) 188–194, <https://doi.org/10.1259/bjr/17790547>.
- [5] K. Ferrara, R. Pollard, M. Borden, Ultrasound microbubble contrast agents: fundamentals and application to gene and drug delivery, *Annu. Rev. Biomed. Eng.* 9 (2007) 415–447, <https://doi.org/10.1146/annurev.bioeng.8.061505.095852>.
- [6] S. Hernot, A.L. Kilbanov, Microbubbles in ultrasound-triggered drug and gene delivery, *Adv. Drug Deliv. Rev.* 60 (2008) 1153–1166, <https://doi.org/10.1016/j.addr.2008.03.005>.
- [7] A. Kheirloomoom, P.A. Dayton, A.F.H. Lum, E. Little, E.E. Paoli, H. Zheng, K.W. Ferrara, Acoustically-active microbubbles conjugated to liposomes: characterization of a proposed drug delivery vehicle, *J. Control. Release* 118 (2007) 275–284, <https://doi.org/10.1016/j.jconrel.2006.12.015>.
- [8] I. Lentacker, S.C. De Smedt, J. Demeester, V. Van Marck, M. Bracke, N.N. Sanders, Lipoplex-loaded microbubbles for gene delivery: a trojan horse controlled by ultrasound, *Adv. Funct. Mater.* 17 (2007) 1910–1916, <https://doi.org/10.1002/adfm.200700106>.
- [9] R. Carlisle, J. Choi, M. Bazan-Peregrino, R. Laga, V. Subr, L. Kostka, K. Ulbrich, C.C. Coussios, L.W. Seymour, Enhanced tumor uptake and penetration of virotherapy using polymer stealthing and focused ultrasound, *J. Natl. Cancer Inst.* 105 (2013) 1701–1710, <https://doi.org/10.1093/jnci/djt305>.
- [10] I. Lentacker, I. De Cock, R. Deckers, S.C. De Smedt, C.T.W. Moonen, Understanding ultrasound induced sonoporation: definitions and underlying mechanisms, *Adv. Drug Deliv. Rev.* 72 (2014) 49–64, <https://doi.org/10.1016/j.addr.2013.11.008>.
- [11] S. Mullick Chowdhury, T. Lee, J.K. Willmann, Ultrasound-guided drug delivery in cancer, *Ultrasonography* 36 (2017) 171–184, <https://doi.org/10.14366/usg.17021>.
- [12] A. Jain, A. Tiwari, A. Verma, S.K. Jain, Ultrasound-based triggered drug delivery to tumors, *Drug. Deliv. Transl. Res.* 8 (2017) 150–164.
- [13] K. Heath Martin, P.A. Dayton, Current status and prospects for microbubbles in ultrasound theranostics, *Wiley. Interdiscip. Rev. Nanomed. Nanobiotechnol.* 5 (2013) 631–637, <https://doi.org/10.1111/j.1747-0285.2012.01428>.
- [14] M.A. Borden, M.R. Sarantos, S.M. Stieger, S.I. Simon, K.W. Ferrara, P.A. Dayton, Ultrasound radiation force modulates ligand availability on targeted contrast agents, *Mol. Imaging* 5 (2006) 139–147, <https://doi.org/10.2310/7290.2006.00016>.
- [15] P. Dayton, A. Kilbanov, G. Brandenburger, K. Ferrara, Acoustic radiation force *in vivo*: a mechanism to assist targeting of microbubbles, *Ultrasound Med. Biol.* 25 (1999) 1195–1201, [https://doi.org/10.1016/S0301-5629\(99\)00062-9](https://doi.org/10.1016/S0301-5629(99)00062-9).
- [16] J. Owen, Q. Pankhurst, E. Stride, Magnetic targeting and ultrasound mediated drug delivery: benefits, limitations and combination, *Int. J. Hyperther.* 28 (2012) 362–373, <https://doi.org/10.3109/02656736.2012.668639>.
- [17] Y. Sheng, E. Beguin, H. Nesbitt, S. Kamila, J. Owen, L.C. Barnsley, B. Callan, C. O'Kane, N. Nomikou, R. Hamoudi, M.A. Taylor, M. Love, P. Kelly, D. O'Rourke, E. Skane, A.P. McHale, J.F. Callan, Magnetically responsive microbubbles as delivery vehicles for targeted sonodynamic and antimetabolite therapy of pancreatic cancer, *J. Control. Release* 262 (2017) 192–200, <https://doi.org/10.1016/j.jconrel.2017.07.040>.
- [18] L.C. Barnsley, M.D. Gray, E. Beguin, D. Carugo, E. Stride, A combined magnetic-acoustic device for simultaneous, coaligned application of magnetic and ultrasonic fields, *Adv. Mater. Technol.* 3 (2018) 1800081, <https://doi.org/10.1002/admt.201800081>.
- [19] C. McEwan, J. Owen, E. Stride, C. Fowley, H. Nesbitt, D. Cochrane, C.C. Coussios, M. Borden, N. Nomikou, A.P. McHale, J.F. Callan, Oxygen carrying microbubbles for enhanced sonodynamic therapy of hypoxic tumours, *J. Control. Release* 203 (2015) 51–56, <https://doi.org/10.1016/j.jconrel.2015.02.004>.
- [20] H.A. Burris, M.J. Moore, J. Andersen, M.R. Green, M.L. Rothenberg, M.R. Modiano, M.C. Cripps, R.K. Portenoy, A.M. Storniolo, P. Tarassoff, R. Nelson, F.A. Dorr, C.D. Stephens, D.D. Von Hoff, Improvements in survival and clinical benefit with gemcitabine as first-line therapy for patients with advanced pancreas cancer: a randomized trial, *J. Clin. Oncol.* 15 (1997) 2403–2413, <https://doi.org/10.1126/science.1198443>.
- [21] H. Nesbitt, Y. Sheng, S. Kamila, K. Logan, K. Thomas, B. Callan, M.A. Taylor, M. Love, D. O'Rourke, P. Kelly, E. Beguin, E. Stride, A.P. McHale, J.F. Callan, Gemcitabine loaded microbubbles for targeted chemo-sonodynamic therapy of pancreatic cancer, *J. Control. Release* 279 (2018) 8–16, <https://doi.org/10.1016/j.jconrel.2018.04.018>.
- [22] N. Nomikou, C. Fowley, N.M. Byrne, B. McCaughan, A.P. McHale, J.F. Callan, Microbubble-sonosensitiser conjugates as therapeutics in sonodynamic therapy, *Chem. Commun. (Camb.)* 48 (2012) 8332–8334, <https://doi.org/10.1039/c2cc33913g>.
- [23] C.A. Sennoga, V. Mahue, J. Loughran, J. Casey, J.M. Seddon, M. Tang, R.J. Eckersley, On sizing and counting of microbubbles using optical microscopy, *Ultrasound Med. Biol.* 36 (2010) 2093–2096, <https://doi.org/10.1016/j.ultrasmedbio.2010.09.004>.
- [24] E. Beguin, L. Bau, S. Shrivastava, E. Stride, Comparing strategies for magnetic functionalisation of microbubbles, *ACS Appl. Mater. Interfaces* 11 (2018) 1829–1840, <https://doi.org/10.1021/acsami.8b18418>.
- [25] C. McEwan, S. Kamila, J. Owen, H. Nesbitt, B. Callan, M. Borden, N. Nomikou, R.A. Hamoudi, M.A. Taylor, E. Stride, A.P. McHale, J.F. Callan, Combined sonodynamic and antimetabolite therapy for the improved treatment of pancreatic

- cancer using oxygen loaded microbubbles as a delivery vehicle, *Biomaterials*. 80 (2016) 20–32, <https://doi.org/10.1016/j.biomaterials.2015.11.033>.
- [26] Y. Chevalier, M.-A. Bolzinger, Emulsions stabilized with solid nanoparticles: pickering emulsions, *Colloids Surf. A Physicochem. Eng. Asp.* 439 (2013) 23–34, <https://doi.org/10.1016/j.colsurfa.2013.02.054>.
- [27] J. Narayanan, J.Y. Xiong, X.Y. Liu, Determination of agarose gel pore size: absorbance measurements vis a vis other techniques, *J. Phys. Conf. Ser.* 28 (2006) 83–86, <https://doi.org/10.1088/1742-6596/28/1/017>.
- [28] E. Stride, C. Porter, A.G. Prieto, Q. Pankhurst, Enhancement of microbubble mediated gene delivery by simultaneous exposure to ultrasonic and magnetic fields, *Ultrasound Med. Biol.* 35 (2009) 861–868, <https://doi.org/10.1016/j.ultrasmedbio.2008.11.010>.
- [29] H. Tajima, I. Makino, Y. Ohbatake, S. Nakanuma, H. Hayashi, H. Nakagawara, T. Miyashita, H. Takamura, T. Ohta, Neoadjuvant chemotherapy for pancreatic cancer: effects on cancer tissue and novel perspectives, *Oncol. Lett.* 13 (2017) 3975–3981, <https://doi.org/10.3892/ol.2017.6008>.
- [30] A. Mitra, B. Sirohi, S.V. Shrikhande, Neoadjuvant therapy in pancreatic cancer, *Curr. Med. Res. Pract.* 4 (2014) 56–61, <https://doi.org/10.1016/J.CMRP.2014.03.002>.